Chemistry–A European Journal
Research Article
doi.org/10.1002/chem.202403861
Chemistry Europe
European Chemical Societies Publishing
www.chemeurj.org

Zinc Sensing with a Pyridine-Based Lanthanide Contrast Agent: Structural Analysis in Aqueous Solution

Harlei Martin,[a] Adrien Uguen,[a] Jean-François Morfin,[a] Manon Isaac,[a] Agnès Pallier,[a] Andrea Melchior,[b] and Célia S. Bonnet*[a]

Zinc is an important physiological cation, and its misregulation is implicated in various diseases. It is therefore important to be able to image zinc by non-invasive methods such as Magnetic Resonance Imaging (MRI). In this work, we have successfully synthesized a novel Gd^{3+}-based complex specifically for Zn^{2+} sensing by MRI. Using a combination of NMR, luminescence, potentiometric, and relaxivity experiments, completed with DFT calculations, we demonstrate that incorporating a short linker between the Zn^{2+} sensing unit and the Gd^{3+} complex leads to unique behavior of the system in the absence of Zn^{2+}. A significant increase in efficacy of the system is observed upon Zn^{2+} binding, and importantly, the complex is highly selective for Zn^{2+} relative to other physiological cations. A comprehensive structural study reliably determines the microscopic parameters at the origin of the Zn^{2+} response, primarily an increase in the number of water molecules directly coordinated to Gd^{3+} upon Zn^{2+} binding. Crucially, the system maintains a strong response to Zn^{2+} binding in the presence of Human Serum Albumin, highlighting its potential for biological applications.

Introduction

For a long time, magnetic resonance imaging (MRI) has been focused on acquiring anatomical and functional images. More recently, a new field called molecular imaging has emerged, aiming to visualise the expression or function of bioactive molecules and acquire information at the molecular level. This technique enables early diagnosis, as biochemical or physiological changes caused by a disease are detectable prior to morphological changes. Specific imaging probes for a given molecular event are required to attain molecular imaging. Gd^{3+}-based MRI contrast agents (CAs) are particularly suitable for the design of responsive probes. For a selective MRI response to a physiological parameter, the efficacy of the probe (called relaxivity) must be modified specifically by the parameter being assessed.[1] Responsive CAs are designed based on changes in one or more factors that control relaxivity, including the number and exchange rate of water molecules coordinated to Gd^{3+}, or the rotational correlation time of the complex. Physiological parameters that can be monitored through MRI include pH,[2] concentration of O_2,[3] enzymatic activities,[4] endogenous ions[5] and biologically relevant small molecules.[6]

Zinc is the second most abundant d-block metal in the body and exists exclusively as the divalent ion (Zn^{2+}). The Zn^{2+} ion is involved in many biological processes, including controlling gene transcription and metalloenzyme function,[7] and therefore the concentration of this ion is tightly regulated by cells. Disturbances in Zn^{2+} homeostasis has been linked to many diseases, such as diabetes,[8] prostate cancer,[9] and neurogenerative diseases like Alzheimer's disease.[10] Hence, it is crucial to monitor Zn^{2+} levels *in vivo* to gain a better understanding of its biological functions and to facilitate early diagnosis of specific pathologies.

The development of MRI contrast agents for molecular imaging, in particular Zn^{2+} detection, requires a change in the state of the contrast agents upon interaction with the biomarker of interest (*ie* Zn^{2+} concentration). The first Zn^{2+} responsive MRI contrast agent was reported in 2001, consisting of a Gd^{3+} DPTA bisamide complex with two DPA units available for Zn-complexation.[11] In recent years, MRI contrast agents sensitive to Zn^{2+} ions have seen tremendous development,[12] including *in vivo* detection.[13] Zn^{2+} responsive probes are typically composed of three main parts: a paramagnetic metal-ion complexing unit (MRI active part), a Zn^{2+} complexing unit, and a linker connecting them . Each of these units has been shown to play a key role in determining the probe's response.[14]

Herein, we report the synthesis and an in-depth potentiometric, structural and relaxometric study of a novel Gd^{3+} complex based on the **PyC1DPA** chelator (Figure 1), providing a thorough understanding of the supramolecular interactions responsible for the Zn^{2+} response. It is compared to previously reported complexes based on similar pyridine ligands (shown in Figure 1). **Py** ligand was proven to form bishydrated Gd^{3+} complexes of high thermodynamic stability and kinetic inert-

[a] Dr. H. Martin, A. Uguen, Dr. J.-F. Morfin, Dr. M. Isaac, A. Pallier, Dr. C. S. Bonnet
Centre de Biophysique Moléculaire
CNRS UPR 4301, Université d'Orléans
Rue Charles Sadron, 45071 Orléans, Cedex 2, France
E-mail: celia.bonnet@cnrs.fr
[b] Prof. A. Melchior
Polytechnic Department of Engineering,
University of Udine
via del Cotonificio 108, 33100 Udine, Italy

Supporting information for this article is available on the WWW under https://doi.org/10.1002/chem.202403861

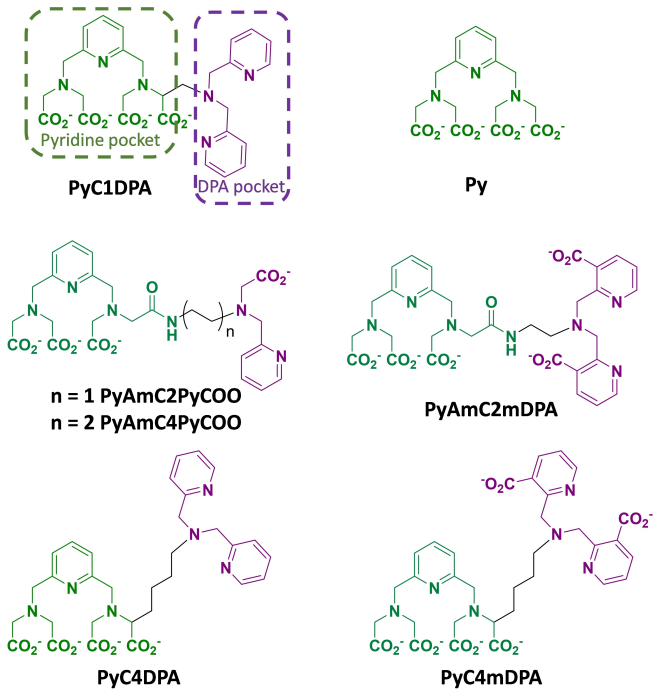

Figure 1. Chemical structures of the ligands discussed in this work.

ness, and showed no *in vitro* or *in vivo* toxicity.[15] It has been demonstrated that physiological anions do not replace the two water molecules present in the first coordination sphere of Gd^{3+}. As a result, this ligand has been developed into Zn^{2+}-responsive probes on the basis that a change of the hydration number from 0 to 2 could be theoretically attained, leading to important changes in the relaxivity upon Zn^{2+} binding. We have already explored several complexes of this family of ligands showing variations in the charge of the Gd^{3+}-binding unit, in the Zn^{2+} binding unit and in the length of the linker (shown in Figure 1). However, none of the corresponding Gd^{3+} complexes responded to Zn^{2+} through a change in the hydration number. The first generation of complexes (Gd**PyAmCxPyCOO**) responded to Zn^{2+} by the formation of a dimeric species.[16] To avoid such dimers detrimental for Zn^{2+} quantification, a second generation of ligands with a modified Zn^{2+} binding unit, based on bis(pyridylmethyl)amine (DPA) (**PyAmC2mDPA**) was synthesized and the corresponding complexes studied. The relaxivity changes upon Zn^{2+} binding is triggered by the presence of Human Serum Albumin (HSA).[17] We also investigated the effect of the charge of the Gd^{3+} complex (Gd**PyC4mDPA**) on this binding.[17] A similar increase in relaxivity in the presence of HSA is observed when using a DPA unit for Zn^{2+} recognition (Gd**PyC4DPA**).[18] A Gd/$^{165}Er^{3+}$-**PyC4mDPA** cocktail allowed the quantitative detection of Zn^{2+} using a combination of MRI and SPECT.[19] The Gd**PyC4mDPA** complex was also used to prove that, *in vivo*, local accumulation due to enhanced HSA affinity is responsible for the Zn^{2+} response.[13a]

To further expand this family of ligands and obtain a change in the hydration sphere of Gd^{3+}, we reasoned that a short linker facilitating strong H-bonding between the "pyridine pocket" and the "DPA pocket" would be suitable, prompting the synthesis of **PyC1DPA**.

The detailed structural characterisation of Gd**PyC1DPA** using potentiometry, luminescence, NMR, relaxometry experiments and DFT calculations highlights the unique behaviour of the complex in its non-hydrated and bishydrated forms at physiological pH. The proportions of each isomer could be determined and showed unambiguously that this behaviour is responsible for the change in relaxivity upon Zn^{2+} binding. Importantly, these changes are highly selective for Zn^{2+} vs other physiological cations, including Cu^{2+}, which is classically difficult to achieve. Finally, the Zn^{2+} response is retained in the presence of HSA.

Results and Discussion

Synthesis of the Ligand

H_4**PyC1DPA** was synthesised in a convergent procedure (Scheme 1). Acid catalysed esterification of commercially available 3-amino-*N*-benzyloxycarbonyl-L-alanine afforded the *tert*-butyl ester compound, which was then reacted with picolyl chloride hydrochloride to give compound **1**. Deprotection of the Cbz-group was carried out using hydrogenation with Pd/C as the catalyst. The free amine was then reacted with *tert*-butyl bromoacetate to give compound **2**. In parallel, monoalkylation of 2,6-di(bromomethyl)pyridine with di-*tert*-butyl iminodiacetate afforded compound **3**. The reaction between **2** and **3** followed by final saponification, afforded protonated ligand H_4**PyC1DPA**.

Protonation Constants of the Ligands and Stability of the Complexes

Potentiometric studies of **PyC1DPA** were performed to determine the species present in solution and their stability constants. The protonation constants were assessed, as defined in equation 1.

$$K_i = \frac{[H_iL]}{[H_{i-1}L][H]} \quad (1)$$

PyC1DPA displays six protonation constants (Table 1, Figure 2). The first three constants correspond to the protonation of amine nitrogen atoms, and the others to carboxylate functions and/or the pyridine units of the DPA. By comparison with the protonation constants of the parent **Py** compound,[15a] and those of **PyC4mDPA**,[17] the first two protonation constants can be attributed to the aliphatic nitrogen of the DPA unit and to the nitrogen of the tertiary amine of the 'pyridine pocket' on the opposite side of the DPA substitution. The lower protonation constant of the nitrogen of DPA can be explained by the shorter linker. The third protonation constant (5.39) can be attributed to the protonation of the remaining nitrogen on the pyridine core. This unexpectedly low value can be explained by

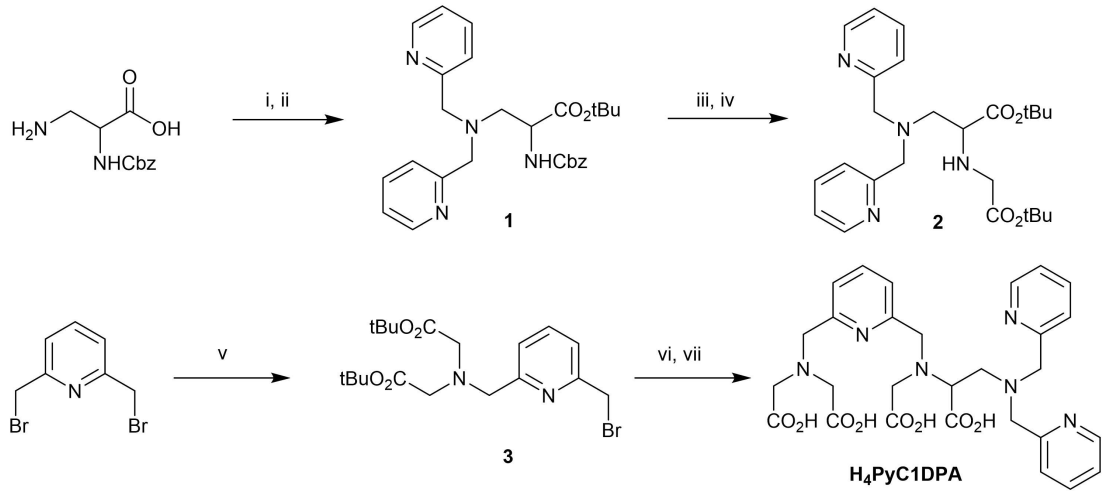

Scheme 1. Synthesis of protonated ligand $\mathbf{H_4L}$. *Reagents and conditions*: (i) $HClO_4$ 65%, *tert*-butyl acetate, rt, 24 h, 62%; (ii) picolyl chloride hydrochloride, K_2CO_3, CH_3CN, 90 °C, 18 h, 59%; (iii) H_2, Pd/C 10%, MeOH, rt, 3 h, 93%; (iv) *tert*-butyl bromoacetate, K_2CO_3, CH_3CN, reflux, 4 h, 84%; (v) di-*tert*-butyl iminodiacetate, K_2CO_3, CH_3CN, 90 °C, 4 h, 76%; (vi) **2**, K_2CO_3, CH_3CN, 90 °C, overnight, 52%; (vii) HCl 4 N, 1,4-dioxane, rt, 4 h, 95%.

Table 1. Protonation constants measured in NaCl 0.15 M at 298 K. The number in bracket indicates the error on the last digit.

Log K_H	PyC1DPA	PyC4mDPA[a]	Py[b]
Log K_{H1}	8.81(1)	10.53(9)	8.95
Log K_{H2}	7.95 (1)	8.75(6)	7.85
Log K_{H3}	5.39 (2)	8.04(4)	3.38
Log K_{H4}	3.90 (3)	3.79(5)	2.48
Log K_{H5}	2.44 (3)	2.81(6)	
Log K_{H6}	1.8 (2)	2.40(9)	
Log K_{H7}		1.9(1)	

[a] in KCl 0.1 M from Ref.[17]. [b] in KCl 0.1 M from Ref.[15a].

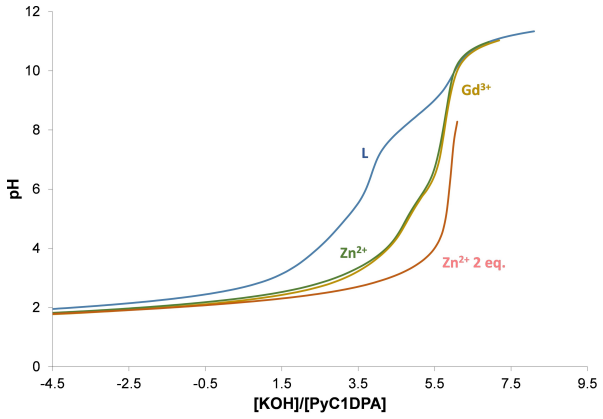

Figure 2. Potentiometric titration curves of solutions containing **PyC1DPA** (2.24 mM) with 0 or 1 equivalents of $ZnCl_2$ and $GdCl_3$ and 2 equivalents of $ZnCl_2$, 0.15 M NaCl, 298 K.

the protonation of the neighbouring DPA nitrogen and the potential for H-bonding, resulting in a stable 5-membered ring. This attribution is supported by the complex's stability and protonation constant (vide infra), as well as the ^{1}H NMR spectra of the ligand at pH 5 and 7 (Figure S1), which show the most significant changes in the chemical shifts of the Hs in the vicinity of this nitrogen (Table S1, H13a and H15). The protonation constant at 3.90 can be attributed to the protonation of the pyridine of the DPA, as evidenced by the presence of a protonation constant in this range for the complex (vide infra) and by the ^{1}H NMR spectra of the ligands at pH 3 and 5, which show maximum changes in the chemical shifts of the DPA protons (Table S1). Finally, the other protonation constants (Log K_{H5} and Log K_{H6}) can be attributed to the protonation of carboxylate functions.

Potentiometric titrations were also performed to determine the complex stability and protonation constants, logK_{ML} and logK_{MLH} (equations 2 and 3) for the lanthanide cations Gd^{3+}, Lu^{3+} and Eu^{3+}, as well as for Zn^{2+} (Figure 2 and S3 in the Supporting Information). The different species formed and their stability constants are summarised in Table 2. For all three lanthanide cations, non-protonated, monoprotonated and diprotonated mononuclear complexes are observed, all with very comparable stability constants. It can however be noted that a small increase in Log *K* is observed from EuL to GdL as was shown previously for other complexes of this family.[20] This increase can be explained by an increasing charge density of the cation as observed for flexible ligand such as EDTA.[21] From GdL to LuL, log *K* remains constant whereas the charge density still increases along the Ln^{3+} series. This can be ascribed to the rigidity of the ligand as compared to EDTA, implying that **PyC1DPA** cannot wrap efficiently around the smaller lanthanide cations. The stability constant of Gd**PyC1DPA** is surprisingly lower than that of the parent pyridine complex, likely due to the proximity of the 'DPA pocket'.

All Ln^{3+} complexes can be monoprotonated and diprotonated on the DPA moiety. The first protonation constant occurs on the aliphatic nitrogen of the DPA, while the second occurs on the nitrogen of the pyridine from the 'DPA pocket'.

Table 2. Complex formation constants and their protonations measured in NaCl 0.15 M at 298 K. The number in bracket indicates the error on the last digit.

Log K_H	PyC1DPA	PyC4mDPA[a]	Py[b]
Log K_{GdL}	16.8(1)	20.1(1)	18.60
Log K_{GdLH}	5.86(1)	8.92(6)	–
Log K_{GdLH2}	4.02(1)	3.74(4)	–
Log K_{GdLH3}	–	2.54(6)	–
Log K_{GdLOH}	11.2(2)	10.88(5)	–
Log K_{LuL}	16.58(2)	–	–
Log K_{LuLH}	5.74(2)	–	–
Log K_{LuLH2}	4.02(1)	–	–
Log K_{LuLOH}	11.1(1)	–	–
Log K_{EuL}	16.66(1)	–	–
Log K_{EuLH}	5.75(1)	–	–
Log K_{EuLH2}	4.10(1)	–	–
Log K_{EuLOH}	11.0(1)	–	–
Log K_{ZnL}	15.90(1)	16.5(1)	15.84
Log K_{ZnLH}	6.10(2)	10.03(9)	3.81
Log K_{ZnLH2}	3.92(2)	4.10(4)	–
Log K_{ZnLH3}	2.89(1)	3.20(7)	–
Log K_{ZnLH4}	–	2.4(1)	–
Log K_{ZnLOH}	11.44(5)	11.6(1)	–
Log K_{Zn2L}	7.4	9.9(1)	–
Log K_{Zn2LH}	–	3.98(7)	–
pGd[c]	15.7	17.3	17.4

[a] in KCl 0.1 M from Ref.[17]. [b] in KCl 0.1 M from Ref.[15a]. [c] Logarithmic concentration of the free gadolinium ion ($pLn = -\log[Ln]_{free}$), calculated for $[Ln] = 10^{-6}$ M and $[L] = 10^{-5}$ M at pH = 7.4.

Surprisingly the second protonation constant is slightly higher in the complex than in the ligand, which can be explained by the structure of the ligand allowing the formation of unique H-bonding networks that differ in the complex. Above pH = 10, the titration curves of the lanthanide complexes all show a deprotonation step, indicating the formation of a monohydroxo complex characterised by the protonation constant K_{MLOH} (equation 4).

$$K_{MmL} = \frac{[M_mL]}{[M_{m-1}L][M]} \quad (2)$$

$$K_{MmLHi} = \frac{[M_mL]}{[M_mLH_{i-1}][H]} \quad (3)$$

$$K_{MLOH} = \frac{[ML]}{[ML(OH)][H]} \quad (4)$$

As two binding sites are present in **PyC1DPA**, the absence of dinuclear Ln^{3+} complexes has been checked by luminescence data on the Eu**PyC1DPA** complex. The evolution of the time-resolved luminescence spectra in a titration of **PyC1DPA** with Eu^{3+} by using an excitation wavelength of 261 nm is shown in Figure S4 in the Supporting Information. The luminescence emission arising from Eu^{3+} increases with the addition of up to one equivalent of Eu^{3+} and then remains constant, confirming the formation of a unique 1:1 Ln/L species.

PyC1DPA forms mono- and dinuclear Zn^{2+} complexes. The stability constant for the mononuclear species is relatively high and very similar to that of Zn**Py**, and therefore corresponds to the complexation of Zn^{2+} in the 'pyridine pocket'. As Zn^{2+} is generally 5 or 6 coordinate, the decrease in the basicity of the nitrogen from the 'pyridine pocket' does not affect the Zn^{2+} complexation constant, conversely to what is observed for Ln^{3+} ions with higher coordination numbers. The mononuclear Zn^{2+} complex shows three protonation constants, which are likely occurring on the aliphatic and pyridinic nitrogen atoms of the DPA unit, as well as on a protonatable group in the 'pyridine pocket', as observed for the parent compound Zn**Py**.[15a] Concerning Zn_2**PyC1DPA**, the stability constant is comparable to that of Zn**DPA** ($\log K_{ZnDPA} = 7.6$),[22] indicating complexation at the DPA site. The slightly lower value of 7.4 could be attributed to the electrostatic repulsion between the two Zn^{2+} cations. Importantly, log $K_{ZnPyC1DPA}$ is lower compared to log $K_{GdPyC1DPA}$ by one order of magnitude, proving the selectivity of the 'pyridine pocket' for Gd^{3+} *vs.* Zn^{2+}.

To assess the speciation, luminescence measurements and relaxivity measurements were performed as a function of pH on the Eu^{3+} and Gd^{3+} complexes, respectively. The results presented in Figure 3 accurately reflect the distribution of species in both sets of data. The luminescence of Eu^{3+} increases with the formation of Eu**PyC1DPAH$_2$** and reaches a maximum when Eu**PyC1DPA** is formed. The relaxivity is highest at low pH ($r_1 = 11.4\ mM^{-1}.s^{-1}$ at pH 3, 60 MHz, 25 °C), and decreases with the formation of Gd**PyC1DPAH** and Gd**PyC1DPA**, attaining a value of $6.75\ mM^{-1}.s^{-1}$ at physiological pH. These changes indicate intriguing behaviour involving a change in the hydration number with the pH. This has prompted us to perform a full structural characterisation of Ln**PyC1DPA**.

Structural Study of LnPyC1DPA

To unravel the structure of Ln**PyC1DPA** complex, a combination of NMR data from the diamagnetic Lu**PyC1DPA** and Y**PyC1DPA** complexes, luminescence measurements from the Eu**PyC1DPA** complex, and DFT calculations were used.

The excitation and emission spectra of the Eu**PyC1DPA** complex as a function of pH are presented Figure S4 and S5. The changes in the intensity of the excitation spectra mirror those of the emission (Figure S5 and S6) suggesting important changes in the coordination sphere of the Ln^{3+} around pH 5. Luminescence lifetime measurements were also recorded in H_2O as a function of pH and the data were best fitted by monoexponential decay up to pH 5, with a lifetime of *ca.* 0.4 ms, and by biexponential decay above pH 5, with lifetimes of *ca.* 0.4 ms and 1.2 ms (Figure 4). Luminescence lifetime measurements performed in D_2O at pH 3 and 7.4 allowed to determine the hydration number of Eu^{3+} using empirical

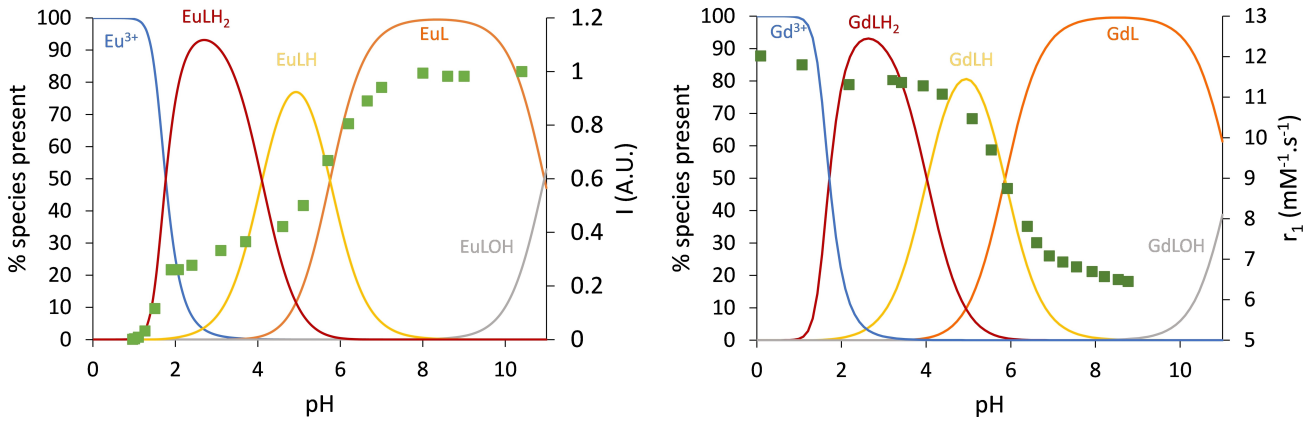

Figure 3. (Left) Normalized luminescence area of the 616 nm band of the Eu^{3+} in the presence of **PyC1DPA** as a function of pH (λ_{exc} = 270 nm) with the species distribution of Eu^{3+} complexes; (Right) Relaxivity measurements of Gd**PyC1DPA** at 60 MHz, 25 °C as a function of pH with the species distribution of Gd^{3+} complexes. Species distribution are calculated from the data in Table 1 and 2.

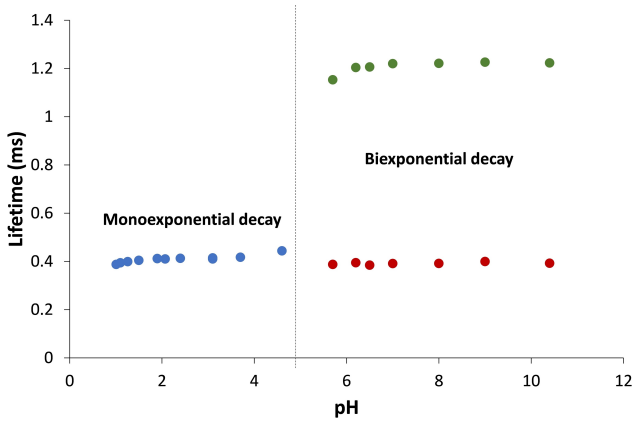

Figure 4. Luminescence lifetime measurements of Eu**PyC1DPA** in H_2O as a function of pH at 298 K.

equations[23] (see Table S3). These results show the presence of a bishydrated species up to pH 5, and an equilibrium between a non-hydrated and a bishydrated species above pH 5. This pH is consistent with the protonation constant of Eu**PyC1DPA** occurring on the tertiary nitrogen atom of the DPA pocket, and consistent with relaxivity and NMR results (vide infra).

To gain a better insight into the structure of these species and their relative concentrations, NMR studies were performed at pD 3, 5 and 7 on the diamagnetic Y^{3+} complex, which serves as a good Gd^{3+} surrogate. 1D and 2D ^1H TOCSY, $^1H/^{13}C$ HMBC, HSQC were systematically recorded for a full attribution of the complexes at different pH. The results are presented in Figure S7 and Tables S4–S5.

At pD 3, two species in slow exchange are present in proportions of 80:20. This is consistent with the proportions of $GdLH_2$ and GdLH observed at this pH (see Figure 3). Normally, such protonation processes are fast on the NMR time-scale, but the presence of H-bonding forming a 5-membered ring in the DPA pocket, where the deprotonation occurs, might slow down this exchange.

At pD 5, again two different species in slow exchange on the NMR time scale are present in proportions of 78:22. Thermodynamic studies indicate that the main species present is YLH (80%) in equilibrium with YL (*ca.* 15%) and YLH_2 (*ca.* 5%). The latter is probably not detectable by NMR due to its low concentration. Since the chemical shifts of the ^1H and ^{13}C for both the major and minor species differ from those observed for YLH at pH 3, this indicates that YLH and YL are in fast exchange on the NMR time-scale, as expected. In the minor species, the two pyridines of the DPA unit are in different chemical environments, as evidenced by their distinct chemical shifts. This is not the case for the major species, where the pyridines of the DPA are equivalent. This suggest the presence of an "open form" that is bis-hydrated, with two equivalent pyridines in the DPA unit that can freely rotate. This form is in slow exchange with a "closed form", where one pyridine coordinates Y^{3+} and the other can freely rotate. The coordination sphere can be completed by the aliphatic amine of the DPA. This "closed form" is non-hydrated, as the DPA coordinates with the cation and expels the water molecules. This attribution is supported by diffusion coefficient measurements and DFT calculations (*vide infra*).

At pD 7, three species are present in slow exchange at the NMR time scale, in proportions of 47:35:18. At this pH, the major species is YL, with less than 6% of YLH present. Chemical shifts analysis shows the presence of an "open form" in 47% and two "closed forms" in 35 and 18%. As previously, it can safely be assumed that the "open form" is bishydrated while the "closed forms" are non-hydrated. The presence of two closed forms can be explained by the presence of several diastereoisomers as there are 3 stereogenic centres on the complex (a CH in the *S* configuration, and two nitrogen atoms coordinated to the Y^{3+}). Compared to pD 5, the percentage of "open form" decreases while that of "closed forms" increases, consistent with the deprotonation of the tertiary amine of the DPA unit, which favours the "closed forms".

The presence of "open" and "closed" forms was also confirmed by diffusion coefficient measurements on the corresponding Lu**PyC1DPA** complex at pD 7, which shows diffusion coefficients of $0.296.10^{-9}$ and $0.320.10^{-9}$ $m^2.s^{-1}$ for the "open" and "closed" forms, respectively (Table S6).

The DFT analysis first confirmed that the minimum energy structure of Eu**Py** (Figure S8) has two coordinated water molecules, which agrees with previous reports of this complex.[15b]

The structure of the [Eu(**PyC1DPA**)$(H_2O)_2$]$^-$ complex, with the DPA moiety coordinated to the metal ion ("closed" form) and uncoordinated ("open" form), obtained by DFT calculations, provides interesting insights into the main conformational isomers of this complex. Two "closed" isomers (A and B Figure 5) differing in the stereochemistry of the N atom next to the chiral carbon were obtained. The main result is that the two water molecules, initially placed near the metal ion, are expelled from the first coordination sphere during the geometry optimization procedure and interact *via* hydrogen bonds with the ligand in the minimum energy structures. In these species, the Eu^{3+} ion is 9-coordinated, with aminic and pyridinic nitrogen atoms (N_{am} and N_{py}) bound to the metal, except for one N_{py} which remains uncoordinated. The average bond lengths obtained for the two isomers are Eu-$N_{am} \approx 2.77$ Å, Eu-$N_{py} \approx 2.69$ Å, and Eu–O ≈ 2.44 Å. Isomer B should be prevalent in solution, as it is 3.0 kcal mol^{-1} lower in energy with respect to A. Thus, an equilibrium between the two forms is likely to be present in solution, as suggested by NMR spectra at pD 7. A higher energy 2 'closed form' was also found (D in Figure S9) where the $N_{am,DPA}$ atom is not coordinated to Eu^{3+}, suggesting that minor percentages of other isomers could be present.

The lowest energy structure of the "open form" (isomer C, Figure 5) is 7.0 and 4.0 kcal/mol higher in energy than B and A, respectively. In this structure, two water molecules are permanently bound to the metal and the N-lone pair of the amine group is orientated to interact via hydrogen bonding with one of them. Another structure (E, Figure S9), differing from isomer C by the orientation of the N-lone pair of the amine group (i.e. the N_{am}-C–C–$N_{am,DPA}$ dihedral angle), has higher energy than C (4.3 kcal mol^{-1}) suggesting that the intramolecular hydrogen bond between the DPA moiety and the coordinated water molecule stabilizes isomer C. Overall, the closed form with no coordinated water molecules is thermodynamically favoured, but an equilibrium between various open and closed isomers is very likely in solution, in accordance with the luminescence and NMR results.

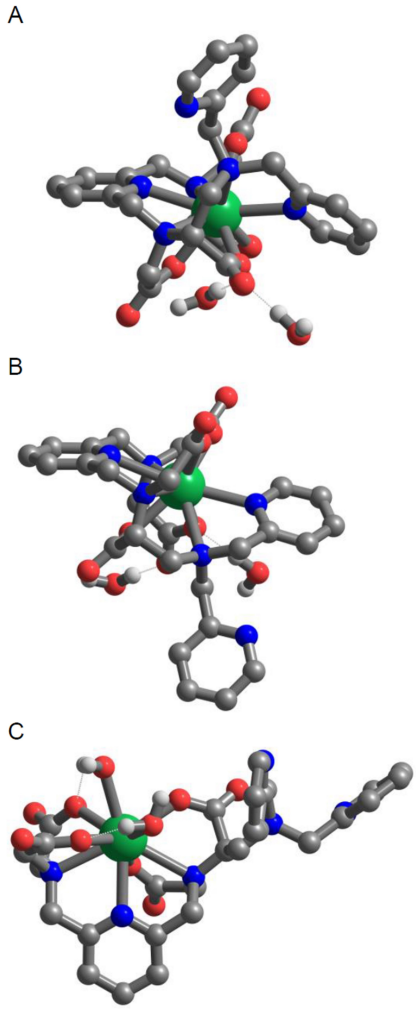

Figure 5. Lowest energy structures of the different isomers of the [Eu(PyC1DPA)$(H_2O)_2$] species.

Relaxometric Response to Zn^{2+}

At physiological pH, the relaxivity of Gd**PyC1DPA** was found to be 6.75 s^{-1}mM^{-1} at 60 MHz and 298 K in HEPES. This is low compared to the bishydrated Gd**PyC4mDPA** (r_1 = 13.8 mM^{-1}.s^{-1}), consistent with the fact that the measured value reflects an average between 47% bishydrated complex and 53% non-hydrated complex (*vide supra*) in these conditions. We anticipated that Zn^{2+} coordination should favour the bishydrated complex, and therefore trigger a relaxivity response at physiological pH. Indeed, upon Zn^{2+} titration at pH 7.4, 60 MHz and 298 K, the relaxivity increases up to 11.10 mM^{-1}.s^{-1} at 0.65 eq. of Zn^{2+} added, and then slightly decreases to reach 10.27 mM^{-1}.s^{-1} at 1 eq. of Zn^{2+} (Figure 6).

The maximum is reached with the addition of 0.65 eq. of Zn^{2+}, which can be explained by two reasons: 1) the formation of dimeric species around Zn^{2+} (Gd**PyC1DPA**)$_2$Zn, and 2) the presence of small aggregates. The formation of Zn(DPA)$_2$

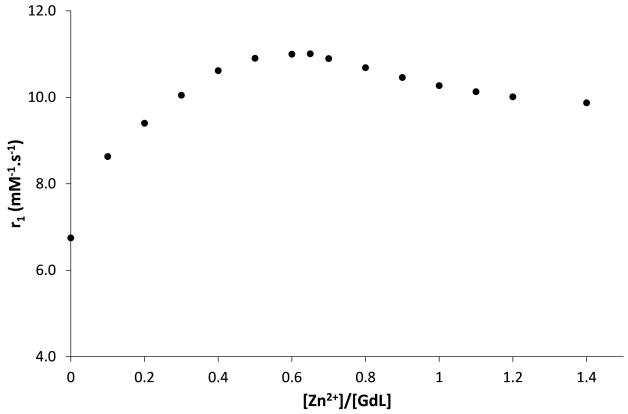

Figure 6. Zn^{2+} titration of Gd**PyC1DPA** at 60 MHz and 298 K in HEPES (0.1 M, 7.4 pH).

species has previously been observed in the literature,[11] and it explains the decrease in relaxivity, corresponding to the formation of Gd**PyC1DPA**Zn, which is smaller in size (with a lower rotational correlation time) than (Gd**PyC1DPA**)$_2$Zn. The presence of the latter is evidenced by potentiometric titrations (Figure S11 and Table S7), which show a formation constant Log $K = 3.85$ for this dimeric species. Moreover, the formation of small aggregates was evidenced by concentration-dependant relaxivity measurements at 0.65 and 1 eq. of Zn^{2+} (Figure S12). Such small aggregates were previously observed for complexes of this family with an ethyl linker, while no aggregates were observed with the butyl linker.[16] This suggests that the presence of a short linker between the Gd^{3+} binding unit and the Zn^{2+} complexing part favours aggregate formation.

Luminescence lifetime measurements were performed on Eu**PyC1DPA** in the presence of various amounts of Zn^{2+} (see Table 3) at 25 °C. It should be noted that similar values were obtained at 50 °C. The results show the presence of non-hydrated and bishydrated species with less than 1 eq. of Zn^{2+}, while only bishydrated species are detected in the presence of 1 eq. of Zn^{2+}, which aligns with the observed increase of relaxivity. This is also consistent with NMR titrations (Figure S13 and S14), which show the presence of free complex in both the "open" and "closed forms" at 0.5 eq. of Zn^{2+} added, whereas only the "open" form is present with 1 eq. of Zn^{2+} added. The ^{1}H NMR spectra of Y**PyC1DPA** with 1 eq. Zn^{2+} show the presence of two species in equilibrium in proportions of 75:25. Similar proportions between these two species are observed at 0.5 eq. of Zn^{2+}, indicating the presence of two isomers in solution, which is consistent with the fact that 3 stereogenic centres are present on the complex as previously seen on the "closed form". The full attribution is given in Tables S8–S9, where both species show non-equivalent pyridine DPA signals, consistent with Zn^{2+} coordination. These species are bishydrated, as indicated by luminescence lifetime measurements (Table 3), and the diffusion coefficient of the corresponding Lu**PyC1DPA**Zn (Table S6) is consistent with that of the "open form" of Lu**PyC1DPA**. The DFT structure of the Zn-containing complex is shown in Figure 7. The Eu^{3+} ion is 9-coordinated with two bound water molecules. On the contrary Zn^{2+} is penta-coordinated, as often found for bivalent metals with tripodal ligands, such as tris(2-pyridylmethyl)amines.[24]

To characterise Gd**PyC1DPA** from a relaxometric perspective, nuclear magnetic relaxation dispersion (NMRD) profiles were recorded in the field range 40 kHz–600 MHz at three

Table 3. Luminescence lifetimes of Eu**PyC1DPA** at physiological pH, 25 °C in H_2O and D_2O, with and without Zn^{2+}, along with the calculated q values.

τ (ms)	τ_1 H_2O	τ_2 H_2O	τ D_2O	q
Eu**PyC1DPA**	0.39(1)	1.14(3)	1.85(7)	$q_1 = 1.9$ (2) $q_2 = 0.0$ (2)
Eu**PyC1DPA** + 0.5 Zn^{2+}	0.39(1)	1.16(2)	1.90(5)	$q_1 = 1.9$ (2) $q_2 = 0.0$ (2)
Eu**PyC1DPA** + 0.65 Zn^{2+}	0.40(1)	1.15(2)	1.88(5)	$q_1 = 1.8$ (2) $q_2 = 0.0$ (2)
Eu**PyC1DPA** + 1 Zn^{2+}	0.39(1)	-	1.93(8)	1.9 (2)

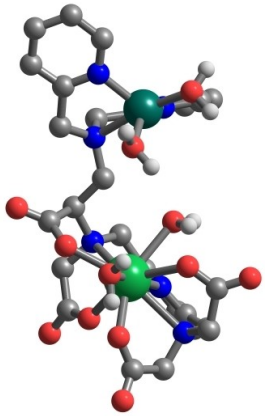

Figure 7. Minimum energy structure of the Zn^{2+} bis-hydrated complex. For clarity, the H atoms attached to carbons and additional non-coordinating water molecules interacting with the complex through hydrogen bonds have been removed (see Figure S10 for the complete structure).

different temperatures (Figure S15), both in the absence and presence of Zn^{2+}. The profiles are typical of small molecular complexes with relaxivity decreasing with temperature, indicating that the rotation is limiting the relaxivity. To determine the microscopic parameters of the complex, these profiles are often combined with ^{17}O NMR spectroscopy. Indeed, variable temperature ^{17}O NMR measurements can give access to the number of water molecules directly coordinated to Gd^{3+} (q), and its exchange rate with the bulk (k_{ex}) through chemical shifts and transverse relaxation rates, respectively. The reduced ^{17}O chemical shifts are directly proportional to the product of q with the complex concentration. The reduced ^{17}O chemical shifts measured at pH 5 (Figure S16), considering the presence of bishydrated/non-hydrated complexes, confirmed the species distribution obtained by NMR (*vide supra*). At pH 7, the reduced ^{17}O chemical shifts were too small to yield reliable results, however the reduced transverse relaxation rates obtained at pH 5 and 7 were consistent (Figure S17), further supporting the species distribution obtained by NMR at these two pH values.

The ^{17}O-reduced transverse relaxation rates of Gd**PyC1DPA** first increase (up to ca. 298 K), then decrease with increasing temperature, indicating that the complex is in the slow kinetic region at low temperatures and in the fast exchange region at higher temperatures. ^{17}O transverse relaxation rates were also measured in the presence of 1 equivalent of Zn^{2+} (see Figure 8), and interestingly the behaviour is quite different, indicating an influence of Zn^{2+} complexation on k_{ex}. This is different than what has been previously observed with complexes in this family bearing an ethyl or a butyl linker[16] and can certainly be ascribed to the shorter linker.

In the presence of 0.65 eq. of Zn^{2+}, a mixture of Zn^{2+} bound and unbound complexes is present, while at 1 eq. of Zn^{2+}, only bound species are present in two isomeric forms. These isomers can theoretically exhibit different water exchange rates, but in this case, the differences between the isomers do not occur around the Ln^{3+} centre. Moreover, the ^{17}O NMR data recorded in the presence of Zn^{2+} provide no evidence of different

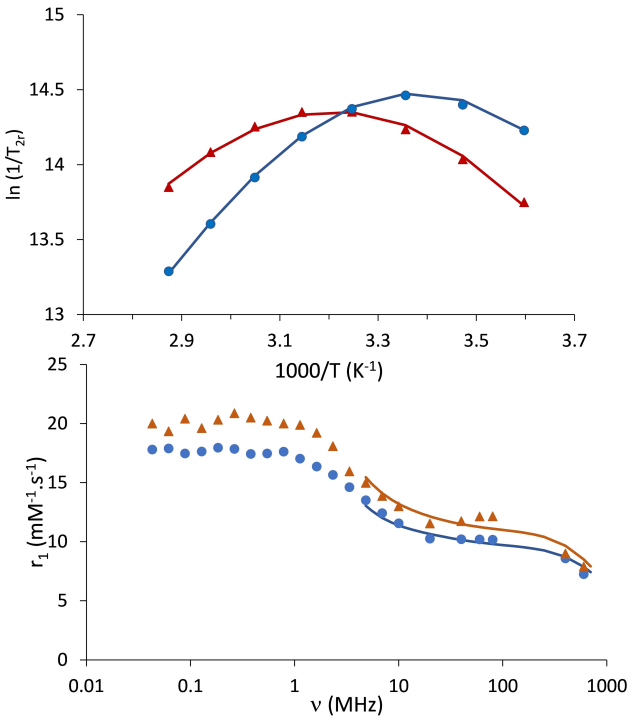

Figure 8. (Top) Temperature dependence of reduced ^{17}O transverse relaxation rates of Gd**PyC1DPA** in the absence (●) and in the presence of Zn^{2+} (▲) at 9.4 T; (Bottom) Calculated NMRD profile of the "open form" of Gd**PyC1DPA** (●) and profile of Gd**PyC1DPA**Zn (▲). The lines represent the fit to the SBM theory using the parameters of Tables 4 and S10.

exchange rates and can be fitted very well assuming a single k_{ex} value.

The ^{17}O relaxation data and the NMRD profiles were analysed with the Solomon-Bloembergen and Morgan (SBM) theory to yield the microscopic parameters characterizing water exchange and rotation (see ESI for equations). We decided to include only relaxivity values above 4.5 MHz in the fitting process as the electron spin relaxation, which is not well described by the SBM theory alone, is then negligible, and the SBM approach gives reliable information on dynamic processes like water exchange and rotational correlation times for small complexes.[25,26]

We fitted the values in the absence and presence of 1 eq. of Zn^{2+} to determine the microscopic parameters of the "open form" of Gd**PyC1DPA** and Gd**PyC1DPA**Zn. To do so, the NMRD profile of the "open form" of Gd**PyC1DPA** was recalculated by subtracting the contribution of the "closed form" (purely outer-sphere), and adjusting its exact concentration (Figures 8 and S18). A simultaneous fit of ^{17}O and NMRD data was performed for Gd**PyC1DPA**, while separate fits were performed for Gd**PyC1DPA**Zn to account for the aggregation process (Figure 8 and S18–19). The parameters resulting from the best fit are presented (Table 4 and S10).

The fit yielded k_{ex} values of $10.5\times10^6\ s^{-1}$ for Gd**PyC1DPA** and $4.1\times10^6\ s^{-1}$ for Gd**PyC1DPA**Zn. The water exchange rate of Gd**PyC1DPA** is close to that of Gd**PyC4mDPA** or Gd**Py** ($9.3\times10^6\ s^{-1}$), as expected. In the presence of Zn^{2+}, this water exchange rate decreases by more than 50%, which can be explained by the close proximity of the Zn^{2+} binding unit, which can interact with the water molecules through hydrogen bonding.

The rotational correlation times of Gd**PyC1DPA**, both in the presence and absence of Zn^{2+}, are similar and consistent with the size of the complexes.

Altogether, this suggests that the Zn^{2+} response is driven by the unique structure of Gd**PyC1DPA** at physiological pH, where it exists as a mixture of open bishydrated and closed non-hydrated forms.

In order to assess the potential of the complex to sense Zn^{2+} selectively, relaxivity changes were determined in the presence of other biologically relevant cations such as Cu^{2+}, Ca^{2+}, and Mg^{2+}. The Gd**PyC1DPA** complex did not exhibit any change in relaxivity when one equivalent of the various cations (Cu^{2+}, Ca^{2+}, Mg^{2+}) were added (Figure 9). This indicates a high selectivity of this complex for sensing Zn^{2+} cations. Most previously reported ligands that are designed to sense Zn^{2+} also sense Cu^{2+} due to their similar recognition motifs. Therefore, this result emphasises the exceptional ability of Gd**PyC1DPA** in detecting selectively Zn^{2+} ions.

Finally, we also looked at the Zn^{2+} response in the presence of HSA, as other complexes from this family were shown to respond to Zn^{2+} in the presence of HSA.[17–18] Gd**PyC1DPA** was titrated against HSA (0–1 mM) both in the absence and presence of Zn^{2+} ions. It was observed that in both cases, the relaxivity increased with increasing HSA concentration, indicating that an interaction is occurring between the complex and the protein (Figure S20). However, due to the presence of

Table 4. Parameters obtained from the fit of the NMRD profiles and ^{17}O data using the SBM theory.

	GdPyC1DPA "open form"	GdPyC1DPAZn	GdPyC4mDPA[a]	Py[b]
q^b	2	2	2	2
k_{ex}^{298} ($10^6\ s^{-1}$)	10.5 (2)	4.1 (1)	9.3	9.3
$\Delta H^{\neq}$ (kJ mol^{-1})	40 (1)	36 (1)	50.4	50.4
E_R (kJ mol^{-1})	25 (1)	18 (1)	21	20.2
τ_R^{298} (ps)	151 (3)	133 (3)	185	92
A/$\hbar$ (10^6rad.s^{-1})	−4.0 (3)	−3.6 (1)	−3.6	−3.7

[a] From ref. [13a]. [b] From ref. [27].

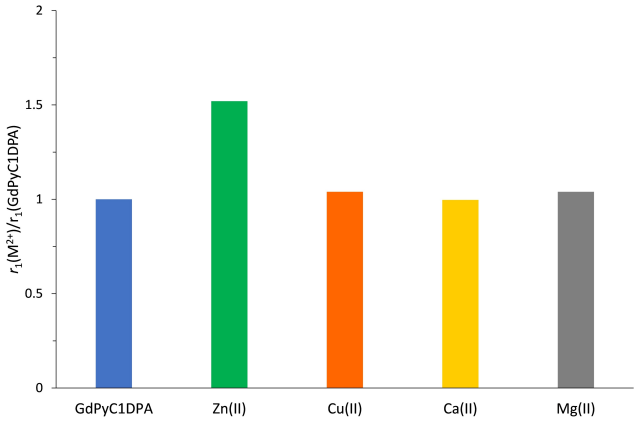

Figure 9. Normalized relaxivity of Gd**PyC1DPA** in the presence of 1 equivalent of various M^{2+} cations at 60 MHz and 298 K in HEPES (0.1 M, 7.4 pH).

several species in solution both in the absence and in the presence of Zn^{2+} under these conditions, it is difficult to extract an affinity constant for HSA. The NMRD profiles of Gd**PYC1DPA** in the presence of physiological concentrations of HSA (0.6 mM) were recorded in the absence and presence of Zn^{2+} at 25 and 37 °C (Figure S21). The characteristic humps, present in both profiles at high field (20–80 MHz), confirms the interaction of the complexes with HSA in the absence and presence of Zn^{2+} and show that a sizeable response by Zn^{2+} addition in the presence of physiological HSA is present.

Conclusions

To conclude, we have synthesized a new Gd^{3+} complex for Zn^{2+} sensing, with a short linker between the Gd^{3+} binding site and the Zn^{2+} sensing unit. Potentiometric titrations show that a stable Gd^{3+} complex is formed, that is selective for Ln^{3+} vs Zn^{2+} and Ca^{2+}. The relaxivity of the Gd**PyC1DPA** complex is highly dependent upon pH, with a pKa value closed to that of the aliphatic amine of the DPA. A full structural study based on NMR and luminescence experiments, completed by DFT calculations, shows the presence of an equilibrium in solution between an "open form" where the Ln^{3+} complex is bishydrated and "closed forms" where the Ln^{3+} complex is nonhydrated. Two closed forms exist in solution due to the presence of two stereogenic centres on the complex. These closed forms are lower in energy than the open form. Upon Zn^{2+} binding, an increase of relaxivity of more than 60% at physiological pH, 60 MHz, and 25 °C is observed. This is explained by the formation of a bishydrated Zn^{2+} complex. In the presence of Zn^{2+} a dimeric species could be evidenced by NMR titrations. The full structural characterization of the system enabled us to determine the microscopic parameters responsible for the observed relaxivity increase, which could be related to the increase in the hydration number of Gd^{3+} in presence of Zn^{2+}. Importantly, the system is highly selective for Zn^{2+} over other physiological cations, and retains a strong response in the presence of HSA. We evidence that supramolecular interactions such as H-bonding gives rise to a unique behavior of the system and we believe that this comprehensive structural study of these ditopic systems will enhance our understanding and facilitate the rationalization of the relaxometric behavior of Gd^{3+}-based responsive probes.

Supporting Information

Synthesis

See supporting information.

Liquid Sample Preparation

Ln(III) solutions were prepared in MilliQ water, and their concentrations determined by complexometric titration in urotropine buffer (pH 5.6–5.8) with standardized EDTA and xylenol orange as the indicator. Ligand purity was assessed by adding excess Zn(II), then titrating uncomplexed Zn(II) with EDTA. Gd(III) complexes were prepared by mixing stoichiometric amounts of $GdCl_3$ with each ligand in HEPES buffer (0.1 M, pH 7.4). Free Gd(III) was tested with xylenol orange, and Gd(III) concentrations were confirmed by ICP-OES and BMS when possible.

Potentiometric Studies

Carbonate-free 0.1 molL^{-1} NaOH and 0.1 molL^{-1} HCl were prepared from Fisher Chemicals concentrates. Potentiometric titrations were performed in 0.1 molL^{-1} aqueous NaCl under nitrogen atmosphere and the temperature was controlled to 25 ± 0.1 °C with a circulating water bath. The p[H] (p[H] = -log[H^+], concentration in molarity) was measured in each titration with a combined pH glass electrode (Metrohm) filled with 3 M KCl and the titrant addition was automated by use of a 702 SM titrino system (Metrohm). The electrode was calibrated in hydrogen ion concentration by titration of HCl with NaOH in 0.1 molL^{-1} electrolyte solution.[28] A plot of meter reading versus p[H] allows the determination of the electrode standard potential (E°) and the slope factor (f). Continuous potentiometric titrations with HCl and NaOH 0.1 molL^{-1} were conducted on aqueous solutions containing 5 mL of **PyC1DPA** 2.24 mM, in NaCl 0.1 molL^{-1}, with 2 minutes waiting between successive points. The titrations of the metal complexes were performed with the same ligand solutions containing 1 or 2 equivalents of metal cation, with 2 minutes waiting time between 2 points. Experimental data were refined using the computer program Hyperquad 2008.[29] All equilibrium constants are concentration quotients rather than activities and are defined as:

$$K_{mlh} = \frac{[M_m L_l H_h]}{[M]^m [L]^l [H]^h}.$$

The ionic product of water at 25 °C and 0.15 molL^{-1} ionic strength is $pK_w = 13.77$.[30] Fixed values were used for pK_w, ligand acidity constants and total concentrations of metal, ligand and acid. All values and errors (one standard deviation) reported are at least the average of three independent experiments.

Temperature-Dependent ^{17}O NMR Measurements

The transverse ^{17}O relaxation rates ($1/T_2$) and the chemical shifts were measured in aqueous solutions of Gd**PyC1DPA** in the temperature range 278–348 K, on a Bruker Avance 400 (9.4 T, 54.5 MHz) spectrometer. The temperature was calculated according to previous calibration with ethylene glycol and methanol.[31] An acidified water solution ($HClO_4$, pH 3.3) was used as external reference. Transverse relaxation times (T_2) were obtained by the Carr-Purcell-Meiboom-Gill spin-echo technique.[32] The technique of the ^{17}O NMR measurements on Gd^{3+} complexes has been described elsewhere.[33] The samples were sealed in glass spheres fitted into 10 mm NMR tubes to avoid susceptibility corrections of the chemical shifts.[34] To improve the sensitivity, ^{17}O-enriched water (10 % $H_2{}^{17}O$, CortectNet) was added to the solutions to reach around 1 % enrichment. The concentrations and pH of solutions were as follows: [Gd**PyC1DPA**] = 11.40 mM at pH = 5 and 11.20 at pH 7.3, with 0; 0.65 and 1 equivalents of Zn^{2+}. The reduced values in the absence of Zn were obtained by taking into account the percentage of open form (two water molecules directly coordinated to Gd^{3+}) and closed form (zero water molecule) at a given pH from the NMR experiments. The ^{17}O NMR data have been treated according to the Solomon-Bloembergen-Morgan theory of paramagnetic relaxation (see Supporting Information). The least-squares fit of the ^{17}O NMR data were performed using Micromath Scientist version 2.0 (Salt Lake City, UT, USA). The reported errors correspond to two times the standard deviation.

NMR Spectroscopy

The NMR spectra were recorded on a Bruker Avance 600 spectrometer equipped with a BBFO probe, and on a Bruker Avance III HD 700 equipped with a CPTCI cryoprobe. The spectra were recorded in D_2O at 4.01 mM (Y**PyC1DPA**), pD = 3.09; and 8.98 mM at pD 5.07 and 7.04 in the absence and in the presence of 0.5 and 1 eq. of Zn^{2+}. ^1H and ^{13}C NMR spectra were recorded at 298 K (otherwise stated). When necessary, a solvent suppression was achieved using an excitation sculpting sequence. ^1H, ^{13}C, TOCSY, NOESY, HSQC and HMBC spectra were systematically recorded. A mixing time of 70 ms, and 300 ms were used for the TOCSY and NOESY experiments, respectively.

Diffusion Coefficient Measurements

The self-diffusion coefficients D^t were measured by applying the bipolar stimulated spin-echo sequence to protons in the complex in D_2O solutions.[35] The proton gyromagnetic ratio is denoted by γ_I, the strength of the gradient pulse by g, the duration of this gradient by δ and the diffusion delay by Δ. The self-diffusion coefficient D^t was calculated by fitting of the theoretical expression of the proton signal intensity $I(\delta,\Delta,g) = I_0\exp[-(\gamma_I g\delta)^2(\Delta-\delta/3)\,D^t]$, in which $I(\delta,\Delta,g)$ and I_0 are the intensities in the presence and absence of the gradient pulses, respectively. The values chosen for δ and Δ in these measurements depend on the magnitude of the diffusion coefficient being measured. For quickly diffusing HOD molecules, the values of δ and Δ were 2 and 100 ms respectively. For the slowly diffusing complex, they were 3 and 200 ms respectively. In the experiments g was increased from 1.8 to 35.3 G.cm^{-1}.

Relaxometric Measurements

Proton NMRD profiles were recorded on a Stelar SMARTracer Fast Field Cycling relaxometer (0.01–10 MHz) and a Bruker WP80 NMR electromagnet adapted to variable field measurements (20–80 MHz) and controlled by a SMARTracer PC-NMR console. The temperature was monitored by a VTC91 temperature control unit and maintained by a gas flow. The temperature was determined by previous calibration with a Pt resistance temperature probe. The longitudinal relaxation rates ($1/T_1$) were determined in water. The least-squares fit of the ^1H NMRD data was performed by using MicroMath Scientist version 2.0 (Salt Lake City, UT, USA). The solutions were made in HEPES buffer (0.1 M) at pH 7.4 and at the following concentrations: Gd**PyC1DPA**: 0.97 mM, Zn^{2+} was added to obtain 0.65 and 1 equivalent. In the presence of HSA 0.6 mM, the concentrations were as follow: [Gd**PyC1DPA**] = 0.161 mM and [Gd**PyC1DPA**Zn] = 0.195 mM. The Zn^{2+} titrations, HSA titrations, and concentration experiments were performed on a Bruker Minispec at 60 MHz and 298 K, except for HSA titration at 310 K.

Luminescence Measurements

Fluorescence spectra were recorded on an Agilent Cary Eclipse Fluorescence spectrophotometer with the following settings: excitation at 260 or 270 nm and emission scanning between 550 and 750 nm at 298 K, or emission fixed at 616 nm and excitation scanning from 200 to 320 nm.

Europium luminescence lifetimes were recorded on an Agilent Cary Eclipse Fluorescence spectrophotometer by recording the decay of the emission intensity at 616 nm, following an excitation at 260 nm. Measurements were performed in H_2O and D_2O solutions. The settings were as follow: gate time: 0.1 ms; delay time: 0.1 ms; flash count: 1; Total decay time: 10 ms; 100 cycles; PMT detector: 550 mV. At least three decay curves were collected for each sample, all lifetimes were analyzed as monoexponential decays and biexponential decays. The reported lifetimes are an average of at least three measurements.

DFT Calculations

All molecular structures of the complexes were obtained by DFT calculations employing the B3LYP functional[36] with the 6–31 + G(d) basis set for all atoms of the ligands. For the Eu atom the MWB52 Stuttgart-Dresden quasi-relativistic pseudopotential and the associated basis set for valence electrons were employed.[37] The same approach was employed to describe the Zn^{2+} ion, when present. Solvent effect was included by employing the polarizable continuum model (PCM).[38] In particular, the possible isomers of [Eu(**PyC1DPA**)$(H_2O)_2]^-$ were studied by optimizing their geometries in PCM water. In the case of Zn-containing complex ([Eu(**PyC1DPA**)Zn$(H_2O)_{10}]^+$), additional water molecules were also introduced for several reasons. First to determine the number of coordinated waters (2/3) to the Zn^{2+} ion, by adding an excess of water molecules. Second, because during preliminary calculations it was found that, one water bound to Eu was being dissociated in some cases (i.e. the Eu remained 8-coordianted). This finding was in contrast with the experimental observation (see above) and second shell waters were added to include explicit hydrogen bonding between the coordinated and second sphere waters. Indeed, this approach led to a 9-coordinated Eu with two bound water molecules. This observation agrees with previous works[39] which pointed out how the inclusion of second shell waters has a significant impact on improving the description of the hydration structure and energetics of Ln^{3+} aqua ions.

In particular, the possible isomers of [Eu(**PyC1DPA**)$(H_2O)_2]^-$ were studied, while additional solvating water molecules were introduced in the Zn-containing complex [Eu(**PyC1DPA**)Zn-$(H_2O)_{10}]^+$.

Acknowledgements

We thank the Mo2ving platform for NMR and mass spectrometry characterisation. We acknowledge the support from The Fondation de la Maison de la Chimie, and the Agence Nationale pour la recherche (grant ANR-22-CE44-0041). This project has received funding from the European Union's Horizon 2020 research and innovation program under the Marie Sklodowska-Curie grant agreement No 898850.

Conflict of Interests

The authors declare no conflict of interest.

Data Availability Statement

The data that support the findings of this study are available in the supplementary material of this article.

Keywords: Molecular Imaging · Zinc · Gadolinium · responsive probe · Magnetic Resonance Imaging

[1] C. S. Bonnet, L. Tei, M. Botta, E. Toth, in *The Chemistry of Contrast Agents in Medical Magnetic Resonance Imaging* (Eds.: A. E. Merbach, L. Helm, E. Toth), John Wiley & Sons, Chichester, **2013**, pp. 343–385.
[2] a) R. Botár, E. Molnár, G. Trencsényi, J. Kiss, F. K. Kálmán, G. Tircsó, *J. Am. Chem. Soc.* **2020**, *142*, 1662–1666; b) H. Lu, A. Chen, X. Zhang, Z. Wei, R. Cao, Y. Zhu, J. Lu, Z. Wang, L. Tian, *Nat. Commun.* **2022**, *13*, 7948.
[3] V. H. Liu, C. C. Vassiliou, S. M. Imaad, M. J. Cima, *Proc. Nat. Acad. Sci.* **2014**, *111*, 6588–6593.
[4] a) D. V. Hingorani, B. Yoo, A. S. Bernstein, M. D. Pagel, *Chem. Eur. J.* **2014**, *20*, 9840–9850; b) C. J. Kombala, S. D. Lokugama, A. Kotrotsou, T. Li, A. C. Pollard, M. D. Pagel, *ACS Sens.* **2021**, *6*, 4535–4544; c) R. Jouclas, S. Laine, S. V. Eliseeva, J. Mandel, F. Szeremeta, P. Retailleau, J. He, J.-F. Gallard, A. Pallier, C. S. Bonnet, S. Petoud, P. Durand, É. Tóth, *Angew. Chem.* **2024**, *n/a*, e202317728.
[5] a) A. J. Surman, C. S. Bonnet, M. P. Lowe, G. D. Kenny, J. D. Bell, É. Tóth, R. Vilar, *Chem. Eur. J.* **2011**, *17*, 223–230; b) C. S. Bonnet, É. Tóth, *Curr. Opin. Chem. Biol.* **2021**, *61*, 154–169; c) K. P. Malikidogo, H. Martin, C. S. Bonnet, *Pharmaceuticals* **2020**, *13*, 436.
[6] a) F. Oukhatar, S. Même, W. Même, F. Szeremeta, N. K. Logothetis, G. Angelovski, É. Tóth, *ACS Chem. Neurosci.* **2015**, *6*, 219–225; b) A. Barandov, S. Ghosh, N. Li, B. B. Bartelle, J. I. Daher, M. L. Pegis, H. Collins, A. Jasanoff, *ACS Sens.* **2020**, *5*, 1674–1682.
[7] M. I. Costa, A. B. Sarmento-Ribeiro, A. C. Gonçalves, *Int. J. Mol. Sci.* **2023**, *24*, 4822.
[8] A. Fukunaka, Y. Fujitani, *Int. J. Mol. Sci.* **2018**, *19*(2), 476.
[9] L. C. Costello, R. B. Franklin, *Arch. Biochem. Biophys.* **2016**, *611*, 100–112.
[10] Z. Xie, H. Wu, J. Zhao, *Neurotoxicology* **2020**, *80*, 112–123.
[11] K. Hanaoka, K. Kikuchi, Y. Urano, T. Nagano, *J. Chem. Soc. Perkin Trans. 2* **2001**, *9*, 1840–1843.
[12] a) A. C. Esqueda, J. A. Lopez, G. Andreu-De-Riquer, J. C. Alvarado-Monzon, J. Ratnakar, A. J. M. Lubag, A. D. Sherry, L. M. De Leon-Rodriguez, *J. Am. Chem. Soc.* **2009**, *131*, 11387–11391; b) J. Yu, A. F. Martins, C. Preihs, V. Clavijo Jordan, S. Chirayil, P. Zhao, Y. Wu, K. Nasr, G. E. Kiefer, A. D. Sherry, *J. Am. Chem. Soc.* **2015**, *137*, 14173–14179; c) A. F. Martins, V. C. Jordan, F. Bochner, S. Chirayil, N. Paranawithana, S. Zhang, S.-T. Lo, X. Wen, P. Zhao, M. Neeman, A. D. Sherry, *J. Am. Chem. Soc.* **2018**, *140*, 17456–17464; d) M. Regueiro-Figueroa, S. Guenduez, V. Patinec, N. K. Logothetis, D. Esteban-Gomez, R. Tripier, G. Angelovski, C. Platas-Iglesias, *Inorg. Chem.* **2015**, *54*, 10342–10350; e) G. Wang, G. Angelovski, *Angew. Chem.* **2021**, *60*, 5734–5738; f) G. Wang, H. Martin, S. Amézqueta, C. Ràfols, C. S. Bonnet, G. Angelovski, *Inorg. Chem.* **2022**, *61*, 16256–16265; g) J. L. Major, R. M. Boiteau, T. J. Meade, *Inorg. Chem.* **2008**, *47*, 10788–10795; h) M. Isaac, A. Pallier, F. Szeremeta, P.-A. Bayle, L. Barantin, C. S. Bonnet, O. Seneque, *Chem. Commun.* **2018**, *54*, 7350–7353; i) K. P. Malikidogo, A. Pallier, F. Szeremeta, C. S. Bonnet, O. Sénèque, *Dalton Trans.* **2023**, *52*, 6260–6266.
[13] a) K. P. Malikidogo, M. Isaac, A. Uguen, S. Même, A. Pallier, R. Clémençon, J.-F. Morfin, S. Lacerda, É. Tóth, C. S. Bonnet, *Chem. Commun.* **2023**, *59*, 12883–12886; b) A. J. M. Lubag, L. M. De Leon-Rodriguez, S. C. Burgess, A. D. Sherry, *PNAS* **2011**, *108*, 18400–18405; c) M. V. C. Jordan, S.-T. Lo, S. Chen, C. Preihs, S. Chirayil, S. Zhang, P. Kapur, W.-H. Li, L. M. De Leon-Rodriguez, A. J. M. Lubag, N. M. Rofsky, A. D. Sherry, *PNAS* **2016**, *113*, E5464–E5471; d) B. Thapa, E. H. Suh, D. Parrott, P. Khalighinejad, G. Sharma, S. Chirayil, A. D. Sherry, *Front. Endocrinol.* **2022**, *12*, 809867.
[14] C. S. Bonnet, *Coord. Chem. Rev.* **2018**, *369*, 91–104.
[15] a) L. Pellegatti, J. Zhang, B. Drahos, S. Villette, F. Suzenet, G. Guillaumet, S. Petoud, É. Tóth, *Chem. Commun.* **2008**, *48*, 6591–6593; b) C. S. Bonnet, F. Buron, F. Caillé, C. M. Shade, B. Drahoš, L. Pellegatti, J. Zhang, S. Villette, L. Helm, C. Pichon, F. Suzenet, S. Petoud, É. Tóth, *Chem. Eur. J.* **2012**, *18*, 1419–1431.
[16] C. S. Bonnet, F. Caille, A. Pallier, J.-F. Morfin, S. Petoud, F. Suzenet, E. Toth, *Chem. Eur. J.* **2014**, *20*, 10959–10969.
[17] K. P. Malikidogo, M. Isaac, A. Uguen, J.-F. Morfin, G. Tircsó, É. Tóth, C. S. Bonnet, *Inorg. Chem.* **2023**, *62*, 17207–17218.
[18] M. Bödenler, K. P. Malikidogo, J.-F. Morfin, C. S. Aigner, É. Tóth, C. S. Bonnet, H. Scharfetter, *Chem. Eur. J.* **2019**, *25*, 8236–8239.
[19] K. P. Malikidogo, I. Da Silva, J. F. Morfin, S. Lacerda, L. Barantin, T. Sauvage, J. Sobilo, S. Lerondel, E. Toth, C. S. Bonnet, *Chem. Commun.* **2018**, *54*, 7597–7600.
[20] C. S. Bonnet, S. Laine, F. Buron, G. Tircso, A. Pallier, L. Helm, F. Suzenet, E. Toth, *Inorg. Chem.* **2015**, *54*, 5991–6003.
[21] W. P. Cacheris, S. K. Nickle, A. D. Sherry, *Inorg. Chem.* **1987**, *26*, 958–960.
[22] J. K. Romary, J. D. Barger, J. E. Bunds, *Inorg. Chem.* **1968**, *7*, 1142–1145.
[23] R. M. Supkowski, W. D. Horrocks, *Inorg. Chim. Acta* **2002**, *340*, 44–48.

[24] C. Bravin, E. Badetti, G. Licini, C. Zonta, *Coord. Chem. Rev.* **2021**, *427*, 213558.
[25] P. H. Fries, E. Belorizky, *J. Chem. Phys.* **2005**, *123*, 124510.
[26] P. Mieville, H. Jaccard, F. Reviriego, R. Tripier, L. Helm, *Dalton Trans.* **2011**, *40*, 4260–4267.
[27] C. S. Bonnet, F. Buron, F. Caille, C. M. Shade, B. Drahos, L. Pellegatti, J. Zhang, S. Villette, L. Helm, C. Pichon, F. Suzenet, S. Petoud, E. Toth, *Chem. Eur. J.* **2012**, *18*, 1419–1431.
[28] A. E. Martell, R. J. Motekaitis, *Determination and use of stability constants*, VCH, **1992**.
[29] P. Gans, A. Sabatini, A. Vacca, *Talanta* **1996**, *43*, 1739–1753.
[30] R. M. Smith, R. J. Motekaitis, A. E. Martell, National Institute of standards and technology ed., NIST Standard Reference Database, **1997**.
[31] D. S. Raiford, C. L. Fisk, E. D. Becker, *Anal. Chem.* **1979**, *51*, 2050–2051.
[32] S. Meiboom, D. Gill, *Rev. Sci. Instrum.* **1958**, *29*, 688–691.
[33] K. Micskei, L. Helm, E. Brucher, A. E. Merbach, *Inorg. Chem.* **1993**, *32*, 3844–3850.
[34] A. D. Hugi, L. Helm, A. E. Merbach, *Helv. Chim. Acta* **1985**, *68*, 508–521.
[35] A. Jerschow, N. Muller, *J. Magn. Reson.* **1997**, *125*, 372–375.
[36] a) C. Lee, W. Yang, R. G. Parr, *Phys. Rev. B* **1988**, *37*, 785–789; b) A. D. Becke, *J. Chem. Phys.* **1993**, *98*, 1372–1377.
[37] M. Dolg, H. Stoll, H. Preuss, *J. Chem. Phys.* **1989**, *90*, 1730–1734.
[38] J. Tomasi, B. Mennucci, R. Cammi, *Chem. Rev.* **2005**, *105*, 2999–3094.
[39] a) J. Kuta, A. E. Clark, *Inorg. Chem.* **2010**, *49*, 7808–7817; b) P. D'Angelo, R. Spezia, *Chem. Eur. J.* **2012**, *18*, 11162–11178.

Manuscript received: October 18, 2024
Accepted manuscript online: December 27, 2024
Version of record online: February 5, 2025